Original Paper

Fouling of heat exchanger surfaces by dust particles from flue gases of glass furnaces

Peter L. M. Mutsaers, Ruud G. C. Beerkens and Henk de Waal
TNO Institute of Applied Physics, Delft (NL)

Fouling by dust particles generally leads to a reduction of the heat transfer and causes corrosion of secondary heat exchangers. A deposition model, including thermodynamic equilibrium calculations, has been derived and applied to describe the deposition (i.e. fouling) process and the nature of the deposition products in a secondary heat exchanger. The deposition model has been verified by means of laboratory experiments, for the case of flue gases from soda-lime glass furnaces. Corrosion of iron-containing metallic materials, caused by the deposition products, has been briefly investigated with the same equipment.

There is a close similarity between the experimental results and model calculations. The largest deposition rates from flue gases on cylindrical tubes in cross-flow configuration, are predicted and measured at the upstream stagnation point. The lowest deposition rates are determined at downstream stagnation point locations. At tube surface temperatures of approximately 520 to 550 K, the fouling rate on the tube reaches a maximum. In this temperature region $NaHSO_4$ is the most important deposition product. This component is mainly formed at temperatures from 470 up to 540 K. The compound $Na_3H(SO_4)_2$ seems to be stable up to 570 K, for even higher temperatures Na_2SO_4 has been found. These deposition products react with iron, SO_3, oxygen and water vapour forming the complex corrosion product $Na_3Fe(SO_4)_3$. $NaHSO_4$, which is formed at tube surface temperatures below 540 K, causes more severe corrosion of iron-containing materials than Na_2SO_4. Maintaining temperatures of the heat exchanger surfaces above 550 to 600 K reduces the fouling tendency and corrosion in case of flue gases from oil-fired soda-lime glass furnaces.

Ablagerung von Staubpartikeln aus Abgasen von Glasschmelzöfen auf Wärmetauscheroberflächen

Ablagerungen von Staubpartikeln in Sekundärwärmetauschern hinter Regeneratoren oder Rekuperatoren haben eine Reduzierung der Wärmeübertragung zur Folge. Ein Staubablagerungsmodell, das thermodynamische Gleichgewichtsberechnungen einschließt, wurde zur Beschreibung der Ablagerungsprozesse und der Ablagerungsprodukte entwickelt und angewendet. Das Modell wurde durch Laborexperimente mit simulierten Rauchgasen von Kalk-Natronglasschmelzöfen getestet. Mit dieser experimentellen Anordnung wurde außerdem die Korrosion von eisenhaltigen metallischen Werkstoffen bestimmt.

Zwischen experimentellen Ergebnissen und Modellberechnungen wurde eine gute Übereinstimmung gefunden. Die höchsten Ablagerungsraten der Rauchgase an den Wärmetauscherrohren für den Fall von Queranströmung finden sich am stromaufwärts gelegenen Staupunkt. Am stromabwärts liegenden Staupunkt wurden sowohl bei den Berechnungen als auch bei den Experimenten die niedrigsten Ablagerungsraten bestimmt. Bei Zylindertemperaturen von 520 bis 550 K sind die Raten sehr hoch, und das Ablagerungsprodukt ist hauptsächlich $NaHSO_4$. Von 470 bis ungefähr 540 K wird $NaHSO_4$ gebildet, bis 570 K ist wahrscheinlich $Na_3H(SO_4)_2$ stabil, und bei höheren Temperaturen bestehen die Staubpartikel hauptsächlich aus Na_2SO_4. Die ersten zwei Produkte werden aus Na_2SO_4 gebildet durch Reaktion mit SO_3 und Wasserdampf und können weiter reagieren mit Eisen, wobei komplexe Korrosionsprodukte wie $Na_3Fe(SO_4)_3$ entstehen. Bei Oberflächentemperaturen der Wärmetauscherrohre unter 540 K entsteht $NaHSO_4$, das eisenhaltige Werkstoffe stärker korrodiert als Na_2SO_4. Deshalb sollten in ölbefeuerten Kalk-Natronglasschmelzwannen diese Temperaturen möglichst oberhalb von 550 bis 600 K liegen.

1. Introduction

Flue gases from glass melting furnaces may contain vaporisation products of the glass melt and products of fossil fuel combustion. Part of the heat content of the flue gases is transferred to the combustion air by means of regenerator or recuperator devices. The flue gas outlet temperatures from regenerators and recuperators are approximately 800 and 1100 K, respectively. There is a considerable potential to employ a secondary heat exchanger at downstream positions from regenerators or especially recuperators. The secondary metallic heat exchanger can be used to preheat air or to generate steam.

Received 17 November 1988.

However, dust or droplet formation takes place caused by condensation of supersaturated components in the cooling flue gases at temperatures between 1300 and 1100 K. These dust particles have diameters between 0.02 and 0.6 μm [1]. In case of soda-lime glass furnaces, the dust particles mainly consist of sodium sulphate (Na_2SO_4). The fouling tendency of secondary heat exchangers by dust particles reduces the possibility of further recuperation of the flue gas heat content. This behaviour of flue gases in secondary heat exchangers is also described for some practical cases by Webb et al. [2]. Flue gases of oil-fired furnaces contain among high SO_2 concentrations also considerable amounts of SO_3 gas. In these SO_3-rich flue gases, sodium pyrosulphate ($Na_2S_2O_7$) or sodium bisulphate ($NaHSO_4$) are

formed below 600 K. $Na_2S_2O_7$ and $NaHSO_4$, especially in the liquid state, cause severe corrosion of the metallic heat transfer surface, which will reduce the lifetime of the heat exchanger. At the same time the sticky properties of $Na_2S_2O_7$ and $NaHSO_4$ will enlarge the fouling tendency of the heat exchanger. This calculation procedure does not account for penetration of the deposition products in pores of the tube materials, assuming smooth metallic surfaces.

Purpose of this study is to obtain a better understanding of the fouling and corrosion processes of secondary heat exchangers. A simulation model (deposition model), derived from literature, has been applied to predict the deposition (fouling) rates and the nature of the deposits as a function of temperature and location on the heat exchanger tube. The deposition model has been experimentally verified on laboratory scale. Furthermore, the corrosion of iron-containing materials, caused by dust deposits from glass furnace flue gases, has been investigated.

2. Theoretical aspects

2.1. Nature of deposits

Kirkbride [3], Williams and Pasto [4], Roggendorf et al. [5] and Beerkens [6] described the chemical changes taking place in flue gases from glass furnaces during cooling. They applied a thermodynamic equilibrium model to estimate the nature of the deposition and condensation products in regenerators and recuperators of glass furnaces. This model is based upon the assumption that the flue gas composition equals the thermodynamic equilibrium composition at every temperature. In this investigation, the thermodynamic equilibrium model was used for the theoretical calculation of the nature of deposits on the heat transfer surfaces of a secondary heat exchanger. More detailed information of the thermodynamic equilibrium calculations is given in [3 to 6].

2.2. Prediction of deposition rates of flue gas condensates

Fouling of heat exchanging surfaces, which are relatively cold compared to the flue gases, is caused by either:

a) mass transfer of gaseous components from flue gases to channel surfaces and condensation of these compounds at the surfaces or

b) mass transport of dust particles from the flue gases towards the heat-exchanging surfaces.

In recuperators and regenerators the mechanism a) of mass transport is the main cause of fouling [6]. The mechanism b) is responsible for the fouling of secondary heat exchangers.

At temperatures below 1000 K the flue gases generally contain condensed material mainly as submicron dust particles or droplets. Deposition of dust particles in the submicron range can take place by the following separately or simultaneously proceeding processes (neglecting electrostatic forces) [7]:

1. gravitational settling;
2. deposition by inertia of the dust particles;
3. interceptional deposition (only important for very rough surfaces);
4. deposition by Brownian diffusion;
5. deposition by thermophoretic forces (thermophoresis for small particles).

In the practical situation of glass furnaces sodium sulphate dust particles in the flue gases have an average diameter of 0.10 to 0.15 µm [1]. The flue gas velocity is about 2 to 10 m/s and the local temperature difference between flue gas and heat exchanger is 100 to 300 K. Because the sodium sulphate dust particles are small (small particle mass), the deposition processes 1. and 2. are negligible. Furthermore, the deposition surface is usually rather smooth. This means that only deposition by Brownian diffusion and deposition by thermophoretic forces have to be considered.

The differential equation describing the stationary concentration field of dust particles, assuming a monodisperse size distribution in the boundary layer of an object submerged by a flue gas flow, is given for the two-dimensional case by Rosner [8]:

$$\underbrace{\varrho u \frac{\partial W_i}{\partial x}}_{\text{I}} + \underbrace{\varrho (V - V_T) \frac{\partial W_i}{\partial y}}_{\text{II III}} = \underbrace{\varrho D_i \frac{\partial^2 W_i}{\partial y^2}}_{\text{IV}} + \underbrace{k_{\text{eff}} \varrho W_i}_{\text{V}}, \qquad (1)$$

where I = convection term x direction; II = convection term y direction; III = pseudo-convection term y direction caused by thermophoresis; IV = diffusion term; V = pseudo-reaction source term caused by thermophoresis.

Here V_T is the pseudo-suction velocity normal to the wall defined by:

$$V_T = \frac{1}{\varrho} \frac{\partial \varrho D_i}{\partial y} + D_i \alpha_{T,i} \frac{\partial \ln T}{\partial y} \qquad (2)$$

and k_{eff} is the pseudo-first order reaction rate coefficient

$$k_{\text{eff}} = \frac{1}{\varrho} \frac{\partial}{\partial y} \left(\varrho D_i \alpha_{T,i} \frac{\partial \ln T}{\partial y} \right). \qquad (3)$$

The terms V_T and k_{eff} account for the diffusion caused by temperature gradients (i.e. thermophoresis) in the boundary layer and can be seen as a kind of

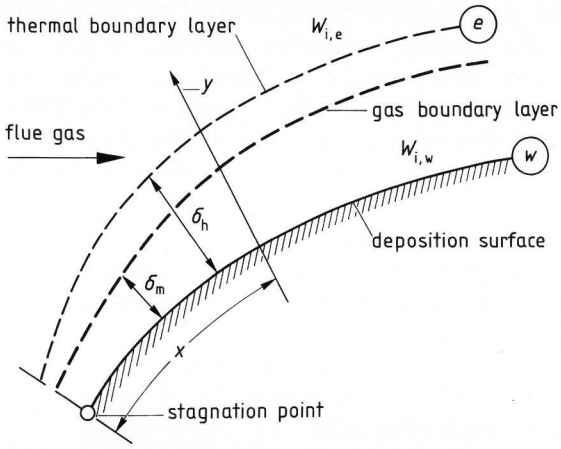

Figure 1. Schematic of boundary layer configuration and related nomenclature. δ_h: thickness of thermal boundary layer, δ_m: thickness of Brownian boundary layer, x, y: coordinates, w: position at the deposition surface, e: position at the thermal boundary layer, W: mass fraction of particles. Subscripts: w = at the surface (wall), e = outer edge of the boundary layer (main stream), i = referring to particles of size class i.

convection term and a kind of first order reaction rate coefficient, respectively.

The direction perpendicular to the deposition surfaces is indicated by y, the direction parallel to this surface (in one direction) is given by the x coordinate, as illustrated by figure 1.

The total mass flux to the wall by Brownian diffusion (first term in equation (4)) and thermophoresis (second term in equation (4)), for particles of size class i, can be written ($W_{i,e} \ll 1$):

$$J_{i,w} = -D_{i,w} \cdot \varrho_w \cdot \left(\frac{\partial W_i}{\partial y}\right)_w \cdot W_{i,w} + \\ + D_{i,w} \cdot \varrho_w \cdot \alpha_{T,i,w} \cdot \left(\frac{\partial \ln T}{\partial y}\right)_w , \qquad (4)$$

where w indicates the position at the deposition surface.

Assuming that, for moderate flue gas velocities, the dust particles in immediate vicinity of the surface stick to the wall, $W_{i,w} = 0$ and the mass flux to the wall is given by the expression given in [8]:

$$J_{i,w} = -D_{i,w} \cdot \varrho_w \cdot \left(\frac{\partial W_i}{\partial y}\right)_w = \varrho_e \cdot St \cdot V_e \cdot W_e . \qquad (5)$$

For high flue gas velocities, the dust particles in the immediate vicinity of the deposition surface, may not completely be adsorbed at this surface, and the sticking efficiency is lower than 100 %, then equation (5) is no longer valid. This means that $W_{i,w} > 0$ and the driving force for dust particle deposition $W_{i,e} - W_{i,w}$ is relatively low compared to the case of a 100 % sticking efficiency. For very high flue gas velocities the value for $W_{i,w}$ reaches the value of $W_{i,e}$ and no deposition takes place.

On the other hand, for increasing flue gas velocities the mass transfer coefficient will increase, thus there is probably an optimal flue gas velocity where deposition of dust reaches a maximum.

The main effect of thermophoresis on the species transport is the influence on the particle concentration profile and thus on $\partial W_i/\partial y$ at the surface: $(\partial W_i/\partial y)_w$.

The Stanton number (ratio of total mass transfer to convective mass transfer) in equation (5) takes into account the mass transfer by Brownian diffusion and the effect of thermophoresis on mass transfer. The calculation of the deposition rates of dust particles is based on a correlation given by Gökoğlu et al. [9]:

$$St = St_0 \cdot \left(\frac{-B_T}{1 - \exp B_T}\right) \cdot \exp(-Da) . \qquad (6)$$

Here St_0 is the Stanton number which includes only mass transfer by convection and Brownian diffusion. This Stanton number is defined as:

$$St_0 = \frac{Sh}{Re \cdot Sc} . \qquad (7)$$

The Sherwood number is a function of the number of Reynolds and Schmidt: $Sh = f(Re, Sc)$. This function depends on the given flow conditions and the obstacle geometry. The calculation of Sh has been thoroughly reviewed in the heat and mass transfer literature [10 and 11].

The function $(-B_T/(1 - \exp B_T))$ is a correction term taking into account the influence of thermophoresis on mass transfer which takes place within the Brownian diffusion boundary layer. B_T is a dimensionless Péclet-like number (ratio of convective to diffusional mass transfer) based on the thermophoretic pseudo-suction velocity, i.e.

$$B_T = (V_T \delta_m)/D_i \qquad (8)$$

which for laminar boundary layers, according to [9], can be expressed as a function of flue gas temperature, surface temperature, thermal diffusivity and Lewis number:

$$B_T = -\alpha_{T,i,w} (Le_w)^{1/3} \left(\frac{T_e - T_w}{T_w}\right) . \qquad (9)$$

The function $\exp(-Da)$ is a correction term taking into account thermophoresis on mass transfer within the thermal boundary layer outside the smaller Brownian diffusion boundary layer. Da is a dimensionless Damköhler number (ratio of pseudo-chemi-

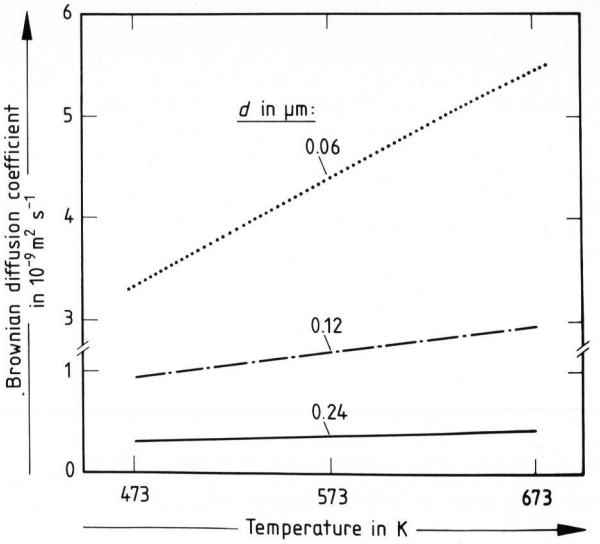

Figure 2. Brownian diffusion coefficient as function of temperature for different diameters of dust particles.

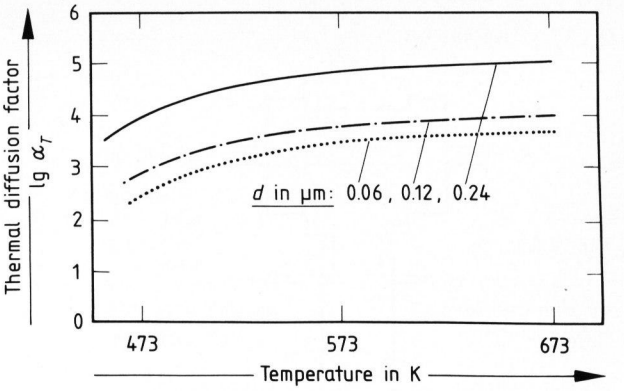

Figure 3. Thermal diffusion factor α_T as function of temperature for Na_2SO_4 dust particles with different diameters.

Table 1. Dependence of parameters C_1, C_2 and C_3 on θ (see equation (11))

θ	C_1	C_2	C_3
0°	0.958	0.54	0.36
30°	0.982	0.52	0.35
60°	0.887	0.49	0.36
90°	0.969	0.37	0.33
120°	1.055	0.18	0.27
150°	0.619	0.23	0.15
180°	0.216	0.58	0.05

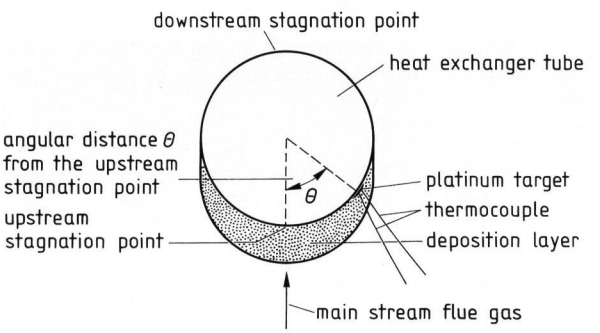

Figure 4. Fouling of a circular heat exchanger tube. θ is the angular distance from the upstream stagnation point.

cal reaction rate to heat diffusivity), based on the thermophoretic pseudo-first order reaction rate coefficient, of the form:

$$Da = \frac{k_{\text{eff}}\,\delta_h^2}{a} \approx \alpha_{T,i,e} \cdot Le_e \cdot \left(\frac{T_e - T_w}{T_w}\right). \qquad (10)$$

The Na_2SO_4 particle transport properties like the Brownian diffusion coefficient and the thermal diffusion factor have been calculated by methods given in [7 and 8], respectively. These values are presented in figures 2 and 3 for three different diameters of Na_2SO_4 particles as a function of the temperature.

The correlation between the local Sherwood number and the numbers of Reynolds and Schmidt, in case of cross-flow configuration, is for a cylinder of the form:

$$Sh_\theta = C_1\, Re^{C_2}\, Sc^{C_3}, \qquad (11)$$

where θ is the angle from the upstream stagnation point (figure 4). The parameters C_1, C_2 and C_3 depending on θ have been derived from Sucker [12] and are given in table 1.

3. Experimental procedure

3.1. Equipment and experimental conditions

Flue gases of a soda-lime glass furnace have been simulated on laboratory scale to investigate the fouling of a secondary heat exchanger. The equipment is illustrated in figure 5. An alumina cylinder with an inner diameter of 5.5 cm is fitted to an air-cooled burner. The burner is fed with propane and air, containing an aspirated sodium sulphate solution. The flue gas from the burner is conducted along a nickel gauze to achieve a more homogeneous distribution of the flue gas. After cooling the flue gas to approximately 900 K, it is mixed with a small amount of air which contains an aspirated sulphuric acid solution. The so obtained SO_3-rich flue gas is conducted into a laboratory scale metal heat exchanger. This procedure has been applied to study the effect of SO_3 on fouling and corrosion by sulphate-rich condensates.

In this heat exchanger the flue gas streams in cross-flow direction along the cylindrical air-cooled heat exchanger tubes. The calculated flue gas composition and the relevant process parameters of the experiments are listed in tables 2 and 3, respectively.

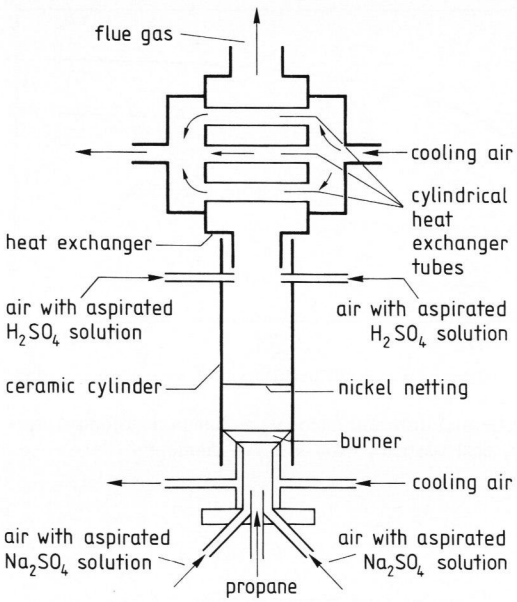

Figure 5. Schematic of laboratory equipment for studying fouling and corrosion of a secondary heat exchanger by simulated flue gases.

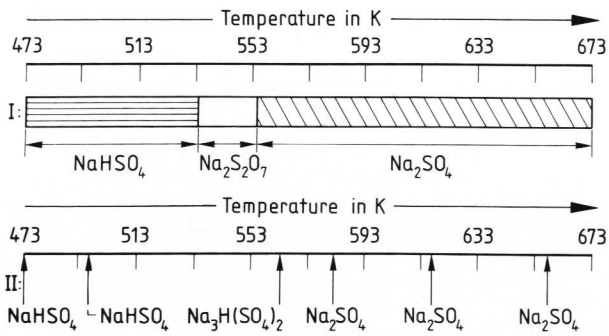

Figure 6. Theoretically and experimentally derived nature of deposition products depending on tube surface temperatures. I = results according to thermodynamic calculations; II = analysis of experimental results at different temperatures.

3.2. Measurement of deposition rates on surfaces of heat-exchanging tubes

Small platinum sheets have been applied to determine the deposition rate as a function of the location on the circular heat exchanger tubes. These platinum sheets were fastened to the tube by means of metal wires. The position of a platinum sheet on the tube is characterized by the angular distance, θ, between the plate and the upstream stagnation point of the tube, as illustrated in figure 4. The amount of deposition product, after a 24 to 28 h lasting experiment, on a platinum sheet is measured by weighing. Thermocouples, welded to the platinum sheets, are used to measure the deposition temperature (i.e. the local surface temperature of a heat exchanger tube).

The nature of the deposition products, which were scraped off the platinum sheets after an experiment, have been determined by means of X-ray diffraction and the concentration of iron and sodium in the deposition or corrosion products were determined by Atomic Absorption Spectroscopy (AAS).

Table 2. Flue gas composition calculated for standard gas conditions (1.013 bar, 273 K)

component	concentration in vol%	concentration in mg / m³
O_2	6.3	–
N_2 + Ar	72.9	–
H_2O	13.0	–
CO_2	7.8	–
SO_3	–	449
Na_2SO_4	–	331

Table 3. Process parameters for the experiments

heat exchanger inlet temperature of flue gas:	750 K
flue gas temperature after the passage of the first heat exchanger tube:	650 K
heat exchanger inlet velocity of flue gas at 750 K:	0.36 m/s
mass fraction of Na_2SO_4 dust particles:	$3 \cdot 10^{-4}$
outer diameter of heat exchanger tubes:	$18 \cdot 10^{-3}$ m

4. Results and discussion

4.1. Comparison of thermodynamic equilibrium calculations with experimental results

The deposition products predicted by the thermodynamic equilibrium model and the experimental deposition products are presented in figure 6 as a function of the tube surface temperature. The experimentally determined deposition product at a tube surface temperature of 564 K, $Na_3H(SO_4)_2$, is not included in the thermodynamic model, because the thermodynamic values (Gibbs free enthalpy) of $Na_3H(SO_4)_2$ are not known from literature. $Na_2S_2O_7$ is possibly an unstable product relative to $Na_3H(SO_4)_2$ for the experimental situations. Above 570 K only sodium sulphate is stable at these flue gas conditions. Below 560 to 570 K other more aggressive sodium sulphates are formed like $NaHSO_4$, $Na_3H(SO_4)_2$ or $Na_2S_2O_7$.

4.2. Comparison of the deposition model calculations with experimentally determined deposition rates

The following assumptions have been made for the calculation of the deposition rate by means of the proposed deposition model:

a) All the Na_2SO_4 dust particles have a diameter of 0.12 µm. This assumption is based on measurements, which were done at industrial soda-lime glass furnaces by Stockham [1].

b) At all tube surface temperatures investigated the dust is assumed to deposit first in the form of Na_2SO_4. Hereafter, Na_2SO_4 can react with components of the flue gas to form the deposition products according to the thermodynamic equilibrium calculations. Formation of the deposition product $Na_3H(SO_4)_2$ is also taken into account.

The experimental and theoretical deposition rates, as a function of the angular distance from the upstream stagnation point of the tube, are presented in figure 7. As shown in this figure, the largest theoretical and experimental deposition rates are determined at the upstream stagnation point and the smallest rates at the downstream stagnation point of the cylindrical tube. According to figure 7 the deposition model calculations agree well with the experimental results.

The experimental and theoretical deposition rates at the upstream stagnation point of the tube depending on the measured tube surface temperature are given in figure 8. From this figure the qualitative agreement between the predicted and experimental deposition rates is shown.

Besides, there is a good quantitative similarity between the theoretical and experimental results, with the exception of the temperature range between 520 and 550 K. A possible explanation for this discrepancy is a change of the particle size in this temperature range. Calculations by means of the model show that both smaller and larger dust particle sizes lead to higher deposition rates. For $d = 0.12$ µm, the deposition seemed to be minimum, this is illustrated in figure 9. Agglomeration of sticky sodium bisulphate condensate particles in this range of experiments may be responsible for larger sizes of the diffusing dust particles and therefore higher deposition rates as expected from the calculations.

5. Corrosion of heat exchanger materials

The corrosion of iron plates, caused by the deposits, has also been investigated with the equipment shown in figure 5. The simulated flue gas composition is the same as given in table 2. The chemical composition of the layer formed on the iron plates was determined by means of X-ray diffraction and AAS. The layer produced at the surface of the iron plates contained mainly Na_2SO_4 and the corrosion product $Na_3Fe(SO_4)_3$. This corrosion product was found at tube surface temperatures between 470 and 670 K.

The highest iron content in the layer was determined at the lower tube surface temperatures: $NaHSO_4$ (deposition product formed below 540 K) causes more corrosion than Na_2SO_4 (deposition product formed above 570 K). At tube surface temperatures below 540 K, the corrosion reaction between $NaHSO_4$, iron and flue gas components is expected to be:

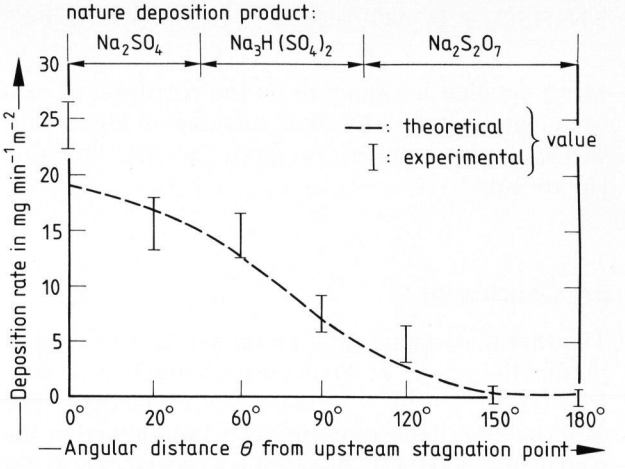

Figure 7. Experimental and theoretical deposition rates as function of the angular distance from the upstream stagnation point of the heat exchanger tube. The tube surface temperatures at the upstream and the downstream stagnation point are 582 and 550 K, respectively.

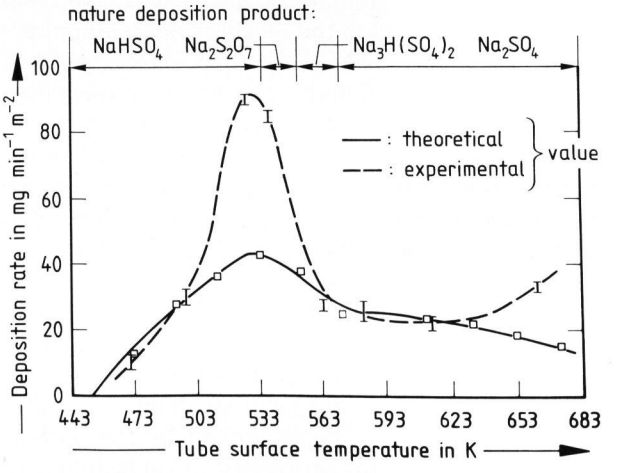

Figure 8. Experimentally and theoretically derived deposition rates at the upstream stagnation point of a cylindrical tube as function of surface temperature.

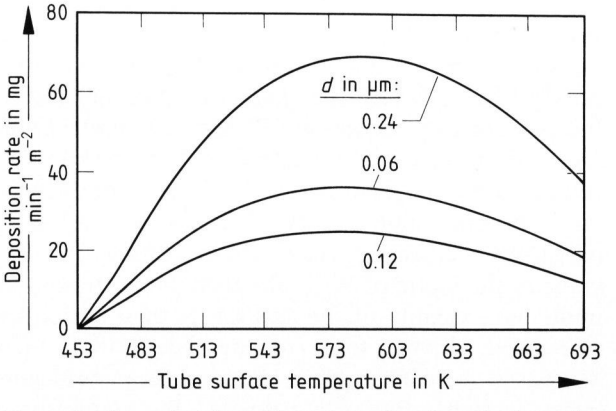

Figure 9. Theoretical deposition rate as function of tube surface temperature for Na_2SO_4 dust particles with different diameters.

$$3\,NaHSO_4 + 1\tfrac{1}{2}\,SO_3 + Fe + \tfrac{3}{4}\,O_2 \longrightarrow Na_3Fe(SO_4)_3 + 1\tfrac{1}{2}\,H_2SO_4\,. \qquad (12)$$

More detailed information on the corrosion of heat exchanger materials by alkali sulphates at higher tube surface temperatures, is given in the literature [13 to 16].

6. Conclusion

The thermodynamic equilibrium model is suitable to predict the nature of the deposition products on heat transfer surfaces of secondary heat exchangers. The experimental deposition products determined in the study are: $NaHSO_4$, $Na_3H(SO_4)_2$, and Na_2SO_4 for SO_3-rich flue gases fom soda-lime glass furnaces. These deposition products cause severe corrosion of iron-containing materials. The corrosion product is mainly $Na_3Fe(SO_4)_3$. $NaHSO_4$, which is formed at tube surface temperatures below 535 K, appears to be more corrosive than Na_2SO_4.

The degree of fouling of heat exchanger tubes depends strongly upon the location and temperature of the tube surface. The largest deposition rates on a cylindrical tube are found at the upstream stagnation point of the tube. At tube surface temperatures of approximately 520 to 550 K maximum fouling of the tubes occurs. There is a good agreement between the experimental results and the calculated deposition rates with the deposition model. Deposition rates have been determined for flue gases flowing through horizontal cylindrical tubes of a boiler behind regenerators of a soda-lime glass furnace with tube temperatures of approximately 400 K. These rates are about 50 mg / (m^3 min) and are comparable with the rates which have been derived by the authors under different circumstances. Application of waste-heat boilers has been demonstrated by Richards [17]. On grounds of the above considerations it can be concluded that the deposition model is a valuable tool to predict the influence of the heat-exchanging surface temperature, the flue gas composition, the flue gas temperature, the flue gas velocity and the geometry of the heat exchanger tubes on the fouling tendency of secondary heat exchangers. For flue gas velocities higher than considered in the present case, equation (5) may not be valid and the deposition of dust particles cannot be directly predicted by the given model. Probably there will be an optimum value of the flue gas velocity with maximum deposition rates. At a certain flue gas velocity the value of $W_{i,w}$, the dust concentration at immediate vicinity of the surface, is then no longer zero. The driving force for dust deposition then decreases and although the mass transfer coefficient increases with flue gas velocity, the diminishing driving force may lead to decreasing deposition rates for even higher velocities.

The size of the dust particles appears to be an important parameter in the model calculations. Accurate measurements of particle-size distributions, depending on flue gas temperature, will approve the applicability of the deposition model.

*

The authors gratefully acknowledge J. W. Visser and E. J. Sonneveld for their extensive X-ray diffraction analysis work.

7. Nomenclature

7.1. Symbols

a	thermal diffusivity of gas in m^2/s
B_T	thermophoretic suction parameter; defined by equations (6 and 8)
c_p	heat capacity of flue gas in J/(kg K)
D	Brownian (Fick) diffusion coefficient for particles in m^2/s
Da	Damköhler number based on k_{eff} (see equations (6 and 10))
k	mass transfer coefficient in m/s
k_{eff}	thermophoretic pseudo-first order reaction rate coefficient in 1/s (see equations (1 and 10))
L	characteristic length in m
Le	Lewis number (ratio of particle Brownian diffusivity to carrier gas heat diffusivity) $Le = D\,\varrho\,c_p/\lambda$
Re	Reynolds number
Sc	Schmidt number
Sh	Sherwood number for mass transfer $Sh = (k \cdot L)/D$
St	Stanton number for mass transfer
T	absolute temperature in K
u	flue gas velocity component parallel to the wall in m/s
V	flue gas velocity component normal to the wall in m/s
V_e	main stream flue gas velocity in m/s
V_T	thermophoretic pseudo-suction velocity normal to the wall in m/s (see equations (1 and 8))
X	stream wise distance along surface in m (see figure 1)
Y	distance normal to the surface in m (figure 1)
W	mass fraction of particles in flue gas
α	$= \lambda/\varrho\,c_P$: thermal heat diffusivity of flue gas in m^2/s
α_T	thermal diffusion factor of particle
δ	boundary layer thickness in m
λ	thermal conductivity of flue glas in J/(s m K)
ϱ	density of flue gas in kg/m

7.2. Subscripts

e	outer edge of the boundary layer (mainstream)
h	outer edge of thermal boundary layer
i	referring to size fraction i
m	outer edge of Brownian diffusion boundary layer
w	at the surface (wall)
o	conditions without thermophoresis

8. References

[1] Stockham, J. D.: The composition of gases evolved from glass furnaces. J. Air Pollut. Control Assoc. **21** (1971) no. 11, p. 713–715.

[2] Webb, R. L.; Marchiori, D.; Durbin, R. E. et al.: Heat exchangers for secondary heat recovery from glass plants. J. Heat Recovery Syst. **4** (1984) no. 2, p. 77–85.

[3] Kirkbride, B. J.: The chemical changes occurring during the cooling of hot gases from flat glass furnaces. Glass Technol. **20** (1979) no. 5, p. 174–180.

[4] Williams, R. O.; Pasto, A. E.: High-temperature chemistry of glass furnace atmospheres. J. Am. Ceram. Soc. **65** (1982) no. 12, p. 602–606.

[5] Roggendorf, H.; Waldecker, G. G.; Scholze, H.: Zusammensetzung der Abgase hinter Glasschmelzwannen. Glastech. Ber. **56** (1983) no. 8, p. 218–227.

[6] Beerkens, R. G. C.: Deposits and condensation from flue gases in glass furnaces. Univ. of Technology Eindhoven (The Netherlands), thesis 1986.

[7] Fuchs, N. A.: The mechanics of aerosols. New York: Pergamon Press 1984.

[8] Rosner, D. E.: Thermal (Soret) diffusion effects on interfacial mass transport rates. PCH, PhysicoChem. Hydrodyn. **1** (1980) no. 2–3, p. 159–185.

[9] Gökoğlu, S. A.; Rosner, D. E.: Correlation of thermophoretically-modified small particle diffusional deposition rates in forced convection systems with variable properties, transpiration cooling and/or viscous dissipation. Int. J. Heat Mass Transfer **27** (1984) no. 5, p. 639–646.

[10] Bird, R. B.; Stewart, W. E.; Lightfoot, E. N.: Transport phenomena. New York: Wiley 1966.

[11] Kays, W. M.; Crawford, M. E.: Convective heat and mass transfer. 2nd ed. New York: McGraw-Hill 1980.

[12] Sucker, D.: Stationärer und instationärer Stoff- und Wärmetransport bei stationär quer angeströmten Zylindern. Tech. Univ. Berlin, Fachbereich 10-Verfahrenstechnik, thesis 1974.

[13] Corey, R. C.; Cross, B. J.; Read, W. T.: External corrosion of furnace wall tubes. Pt. 2//Significance of sulfate deposits and sulfur trioxide in corrosion mechanism. Trans. Am. Soc. Mech. Eng. **67** (1945) p. 289–302.

[14] Jackson, P. J.; Duffin, A. C.: Laboratory studies of the deposition of alkali-metal salts from flue gas. In: Boyland, J. F. (ed.): Mechanism of corrosion by fuel impurities. Proc. Int. Conf. Marchwood 1963. London: Butterworth 1963. p. 427–442.

[15] Raask, E.: Reactions of coal impurities during combustion and deposition of ash constituents on cooled surfaces. In: Boyland, J. F. (ed.): Mechanism of corrosion by fuel impurities. Proc. Int. Conf. Marchwood 1963. London: Butterworth 1963. p. 145–154.

[16] Adams, A. M.; Raask, E.: Complex sulphates in coal-fired boiler deposits. In: Boyland, J. F. (ed.): The mechanism of corrosion by fuel impurities. Proc. Int. Conf., Marchwood 1963. London: Butterworth 1963. p. 496–507.

[17] Richards, B. E.: Waste-heat boilers for flat glass furnaces. In: Smothers, W. J. (ed.): Glass Problems 40//Coll. papers 40th Ann. Conf. Glass Problems, Urbana-Champaign, IL (USA) 1979. p. 50–58.

89R0556